Highly sensitive polymer photodetectors with a wide spectral response range*

Mile Gao(高米勒), Wenbin Wang(王文斌), Lingliang Li(李凌亮),
Jianli Miao(苗建利), and Fujun Zhang(张福俊)†

Key Laboratory of Luminescence and Optical Information of Ministry of Education, Beijing Jiaotong University, Beijing 100044, *China*

(Received 5 August 2016; revised manuscript received 31 October 2016; published online 22 December 2016)

A series of highly sensitive polymer photodetectors (PPDs) was fabricated with P3HT$_{100-x}$:PBDT-TS1$_x$:PC$_{71}$BM$_1$ as the active layers, where x represents the PBDT-TS1 doping weight ratio in donors. The response range of PPDs can cover from the UV to near-infrared regions by adjusting the PBDT-TS1 doping weight ratio. The best external quantum efficiency (EQE) values of ternary PPDs with P3HT:PBDT-TS1:PC$_{71}$BM (50:50:1 wt/wt/wt) as the active layers reach 830%, 720%, and 330% under 390-, 625-, and 760-nm light illumination and −10 V bias, respectively. The large EQE values indicate that the photodetectors utilise photomultiplication (PM). The working mechanism of PM-type PPDs can be attributed to interfacial trap-assisted hole tunnelling injection from the external circuit under light illumination. The calculated optical field and photogenerated electron volume density in the active layers can well explain the EQE spectral shape as a function of the PBDT-TS1 doping weight ratio in donors.

Keywords: conducting polymers, photodetectors, photomultiplication

PACS: 82.35.Cd, 85.60.Gz, 85.60.Ha **DOI:** 10.1088/1674-1056/26/1/018201

1. Introduction

Polymer photodetectors (PPDs) have attracted considerable attention because organic materials have easily adjustable bandgaps and high extinction coefficients.[1–5] However, most PPDs are based on the photovoltaic (PV) effect with the photocurrent originating from exciton dissociation. The external quantum efficiency (EQE) of PV-type photodetectors is less than 100% owing to the limited photon harvesting efficiency, exciton dissociation efficiency, charge carrier transport, and collection efficiency.[6–8] In addition to the EQE values, low dark current (J_D) is also considered a key parameter for evaluating the performance of PPDs because photodetectors should be in a turn-off state in dark conditions.[9–11] For practical application of PV-type photodetectors, a preamplifier is needed to increase the photodetector detectivity (D^*) for weak light, which makes the design and application more complex. Photomultiplication-type (PM–type) photodetectors may be potential candidates to realise weak light detection without preamplifier. Recently, we reported PM-type PPDs based on poly(3-hexylthiophene) (P3HT):[6,6]phenyl-C71-butyric acid methyl ester (PC$_{71}$BM) (100 : 1 wt/wt) as the active layer.[12,13] The working mechanism is attributed to interfacial trap-assisted hole tunnelling injection from the external circuit.

For inorganic photodetectors or photomultiplier tubes, EQE > 100% can be easily realized based on the photoelectron emission effect, impact ionization triggered by hot carriers, or the secondary emission of electrons under high bias (> 100 V).[14,15] However, it is impossible to generate hot carriers in organic films owing to their disordered structures and large binding energy.[16,17] Hiramoto et al. first reported PM-type PPDs in perylene pigment film sandwiched by Au electrodes, which is ascribed to electron injection from the Au electrode to the perylene film assisted by photogenerated hole accumulation near the Au/perylene interface.[18] Yang *et al.* also successfully achieved PM-type organic/inorganic hybrid photodetectors (OIPDs) with inorganic nanoparticles (CdTe) placed into P3HT:[6,6]-phenyl-C61-butyric acid methyl ester (PC$_{61}$BM) (1:1 wt/wt) as active layers.[19] Huang's group successfully fabricated PM-type UV or UV–visible OIPDs based on ZnO nanoparticles blended with P3HT or poly N-vinylcarbazole as an active layer.[20] These results demonstrate that the spectral response range of PPDs can be broadened to the near-infrared (NIR) or UV region by doping different bandgap materials (so-called ternary PPDs). In this work, the narrow-bandgap polymer 2,6-bis(trimethylstannyl)-4,8-bis(5-(octylthio)-thiophen-2-yl)benzo[1,2-b:4,5-b']-dithiophene (PBDT-TS1) was selected as the second donor material to harvest low-energy photons in NIR range. A series of PPDs was fabricated with P3HT$_{100-x}$:PBDT-TS1$_x$:PC$_{71}$BM$_1$ as the active layers, where x represents the PBDT-TS1 doping weight ratio in donors. The EQE values and spectral shape of PPDs could be easily adjusted by changing the PBDT-TS1 doping ratio. For ternary PPDs with P3HT$_{50}$:PBDT-TS1$_{50}$:PC$_{71}$BM$_1$ as active layers,

*Project supported by the Fundamental Research Funds for the Central Universities of China (Grant No. 2014JBZ017) and the National Natural Science Foundation of China (Grant Nos. 61377029 and 61675017).

†Corresponding author. E-mail: fjzhang@bjtu.edu.cn

© 2017 Chinese Physical Society and IOP Publishing Ltd

the spectral response range covers from 350 to 800 nm. The best EQE values are 830%, 720% and 330% under 390-, 625-, and 760-nm light illumination and −10 V bias, respectively.

2. Experiment

The glass substrates coated with indium tin oxide (ITO) (purchased from Shenzhen Jinghua Display Co., Ltd) with a sheet resistance of 15 Ω/square were consecutively cleaned in ultrasonic baths containing detergent, deionised water and ethanol. The cleaned ITO glass substrates were then dried with high-purity nitrogen gas and treated with oxygen plasma for 1 min to improve their work function and clearance. Poly-(3,4-ethylenedioxythiophene)-poly-(styrenesulfonate) (PEDOT:PSS) was spin-coated onto the cleaned ITO glass substrates to prepare an ultrathin anode buffer layer at a spin speed of 5000 rounds per minute (rpm) for 40 s. Then the PEDOT:PSScoated ITO substrates were baked at 120 °C for 10 min under ambient conditions. Polymer P3HT (purchased from Luminescence Technology Corp.), PBDT-TS1 (purchased from Organtec Materials, Inc) and $PC_{71}BM$ (purchased from Luminescence Technology Corp.) were dissolved in 1,2-dichlorobenzene (*o*-DCB) to prepare 40, 25 and 10 mg/mL solutions, respectively. The solutions were continuously stirred at 80 °C for about 12 h. The mixed solutions were prepared with different doping weight ratios of P3HT:PBDT-TS1:PCBM from 100:0:1, 90:10:1, 70:30:1, 50:50:1, 30:70:1, 10:90:1 to 0:100:1, respectively. The mixed solutions were spin-coated onto the PEDOT:PSS layers at 800 rpm for 30 s, forming ∼ 230-nm-thick active layers. The 100 nm thick aluminium (Al) was thermally evaporated on the active layers with a shadow mask in a highvacuum (10^{-5} Pa) chamber. The active area of PPDs is ∼ 3.8 mm^2 which is defined by the vertical overlap of the Al cathode and the ITO anode.

The current density versus voltage (*J*–*V*) curves of all PDDs were measured with a Keithley 2400 source meter under 625- and 760-nm light illumination with light intensity of 8.07 and 5.94 μW/cm^2, respectively. The monochromatic light was provided by a 150-W xenon lamp coupled with a monochromator. The monochromatic light intensity and wavelength were monitored and calibrated by using a Thorlabs S120VC power meter. The absorption spectra of the active layers were measured with a SHINADZU UV-3101 PC spectrophotometer. The optical constants (refractive index (*n*) and extinction coefficients) of the materials used were measured with a SE200BM-M100 spectroscopic ellipsometer (Angstrom Sun Technologies Inc.). The thickness of the active layers was measured with a AMBIOS Technology XP-2 stylus profilometer. All the measurements were conducted at room temperature in ambient conditions. The chemical structure of materials used and a schematic diagram of the device structure are shown in Fig. 1.

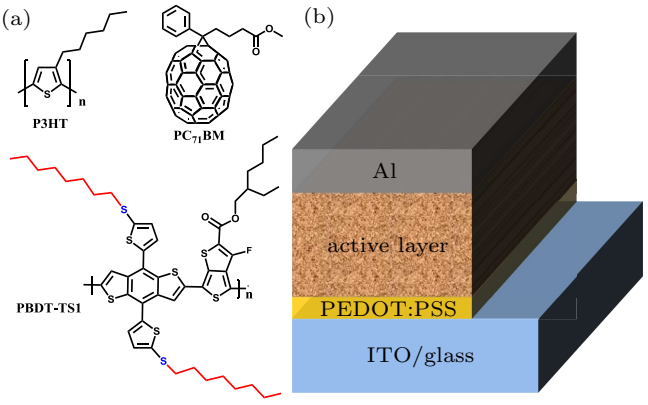


Fig. 1. (color online) (a) Chemical structures of the materials used: P3HT, $PC_{71}BM$, and PBDT-TS1. (b) Schematic diagram of the device structure.

3. Results and discussion

The EQE spectra of PPDs with $P3HT_{100-x}$:PBDT-$TS1_x$:$PC_{71}BM_1$ as active layers were measured under −10 V bias and are shown in Fig. 2(a). It is apparent that the EQE spectral range of PPDs is markedly extended to the NIR by doping PBDT-TS1 in the active layer. Meanwhile, EQE values of PPDs also decreased along with the increase of PBDT-TS1

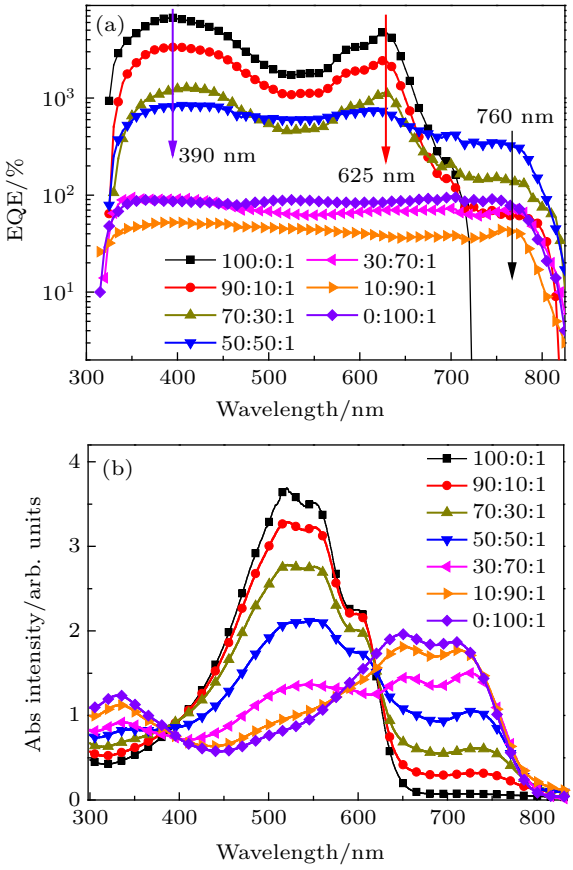


Fig. 2. (color online) (a) EQE spectra of all PPDs with $P3HT_{100-x}$:PBDT-$TS1_x$:$PC_{71}BM_1$ as an active layer ($x = 0$, 10, 30, 50, 70, 90, and 100) under −10 V bias. (b) Absorption spectra of the corresponding $P3HT_{100-x}$:PBDT-$TS1_x$:$PC_{71}BM_1$ films.

doping ratio in donors. For PPDs with PBDT-TS1 doping ratios < 50 wt% in donors, EQE values are $> 100\%$ between 350 and 700 nm. For PPDs with 50 wt% PBDT-TS1 doping ratio in donors, the EQE spectral shape is almost flat and the response range can be extended to 800 nm. The EQE spectral shape of PPDs becomes flatter along with increasing PBDT-TS1 doping ratio. For PPDs with P3HT:PC_{71}BM (100 : 1 wt/wt) as the active layer, the EQE spectra exhibit a distinct dip between 490 and 570 nm, in accordance with the strong absorption range of P3HT:PC_{71}BM (100 : 1 wt/wt) blend film, as exhibited in Fig. 2(b). The underlying reason can be attributed to the weakened hole tunnelling injection induced by the less trapped electrons in PC_{71}BM near the Al cathode.[12,13] The peak EQE values of PPDs with P3HT:PC_{71}BM (100 : 1 wt/wt) as the active layer are 6700% and 4750% at -10 V bias under 390- and 625-nm light, respectively. The EQE values of PPDs markedly decrease with the increase of PBDT-TS1 doping ratio in donors under the same reverse bias, which may be attributed to the disrupted hole transport channels and the shallower electron trap of PC_{71}BM surrounded by PBDT-TS1. Meanwhile, the dip in the EQE spectra of PPDs becomes shallower with decreasing P3HT doping ratio in donors. This means that more photons with wavelengths between 490 and 570 nm can be harvested by the P3HT near the Al electrode in the active layer, resulting in more trapped electrons in PC_{71}BM close to the Al electrode for better hole tunnelling injection from the external circuit. The EQE values of PPDs are significantly enhanced in the long-wavelength range for PBDT-TS1 doping ratios in donors up to 50 wt%, but then decrease for higher PBDT-TS1 doping ratios. The best EQE values reach 830%, 720%, and 330% under 390-, 625-, and 760-nm light illumination, respectively, for optimised ternary PPDs with P3HT:PBDT-TS1:PC_{71}BM (50:50:1 wt/wt/wt) as the active layer at -10 V bias, indicating that the ternary strategy may have great potential for obtaining high-performance NIR PPDs.[21] The extended spectral response range of the optimised PPDs accords well with the absorption spectra of the corresponding blend films, as exhibited in Fig. 2(b).

Clarifying the underlying reason for why PBDT-TS1 doping ratio in donors affects the performance of PPDs entails a discussion on electron trap depth and hole mobility in the active layers. Three kinds of electron traps (P3HT/PC_{71}BM/P3HT, P3HT/PC_{71}BM/PBDT-TS1 and PBDT-TS1/PC_{71}BM/PBDT-TS1) can be formed in the active layers with different PBDT-TS1 doping ratios in donors. The corresponding energy levels of the materials used and the electron trap depth are depicted in Figs. 3(a)–3(c). For the P3HT/PC_{71}BM/ P3HT system, the deeper electron traps form

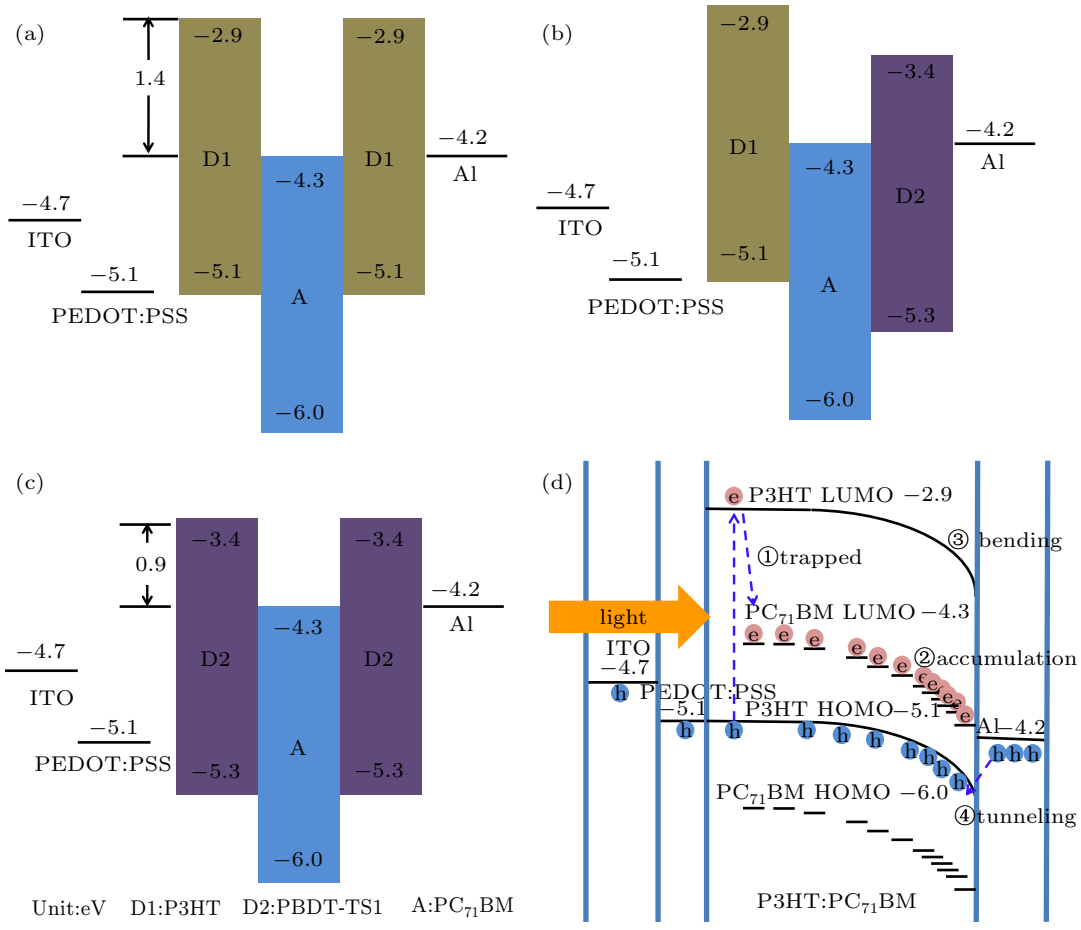


Fig. 3. (color online) Three kinds of electron traps for PC_{71}BM surrounded by (a) P3HT, (b) P3HT/PBDT-TS1, and (c) PBDT-TS1; (d) process of trap-assisted hole tunnelling injection from the external circuit.

as a result of the relatively large energy barrier of 1.4 eV between the lowest unoccupied molecular orbital (LUMO) levels of P3HT and $PC_{71}BM$. For the PBDT-TS1/$PC_{71}BM$/PBDT-TS1 system, the shallower electron traps form as a result of the relatively small energy barrier of 0.9 eV between the LUMO levels of PBDT-TS1 and $PC_{71}BM$. The asymmetric electron traps are formed as a result of $PC_{71}BM$ being surrounded by P3HT and PBDT-TS1. The PBDT-TS1 doping ratio influences the number of electron traps in the active layers. It is apparent that the deeper electron trap formed by P3HT/$PC_{71}BM$/P3HT can trap more electrons, which is beneficial to interfacial band bending owing to the strong Coulomb force induced by the additional trapped electrons. Therefore, holes can be easily injected from the external circuit as a result of the interfacial band bending. Figure 3(d) depicts the process of trap-assisted hole tunnelling injection from the external circuit in PM-type PPDs. The dynamic PM process can be summarised as follows: (i) photon harvesting and exciton dissociation; (ii) photogenerated electrons accumulation in $PC_{71}BM$ near the Al electrode under reverse bias; (iii) interfacial band bending induced by trapped electrons in $PC_{71}BM$ near the Al electrode; and (iv) interfacial trap-assisted hole tunnelling injection from the Al electrode. It is apparent that the EQE values of PPDs with P3HT:$PC_{71}BM$ (100 : 1 wt/wt) as the active layer are much larger than those of PPDs with PBDT-TS1:$PC_{71}BM$ (100 : 1 wt/wt) as the active layer under the same reverse bias. This can be well explained by the hole injection barrier and electron trap depth in the active layer. The highest occupied molecular orbital (HOMO) levels of P3HT and PBDT-TS1 are ~ 5.1 and ~ 5.3 eV, respectively. The hole injection barrier from the Al electrode is 1.8 eV onto the HOMO level of P3HT or 2.0 eV onto the HOMO level of PBDT-TS1 in dark conditions. Meanwhile, because there the fewer electrons in the shallower traps formed by PBDT-TS1/$PC_{71}BM$ /PBDT-TS1, it is difficult to induce more interfacial band bending for hole tunnelling injection from the Al electrode onto the HOMO of PBDT-TS1.

To further confirm our speculation, the optical field distribution and photogenerated electron volume density in the active layer were simulated by using the transfer matrix method.[22–24] The corresponding optical field distribution in the typical blend films are shown in Figs. 4(a), 4(c), and 4(e). In the optical field distribution images, the red region represents a strong optical field caused by interference between incident and reflected light from the Al electrode. The photogenerated electron volume density in the active layer can be estimated according to

$$\rho(\lambda) \propto \frac{|E(\lambda)|^2}{h\nu} \times \eta_{\mathrm{A}}(\lambda) \times \eta_{\mathrm{D}}, \tag{1}$$

where $\rho(\lambda)$ is the photogenerated electron volume density, $|E(\lambda)|^2$ is the optical field intensity, $\eta_{\mathrm{A}}(\lambda)$ is the absorption coefficient, and η_{D} is the exciton dissociation coefficient. The distribution of $PC_{71}BM$ molecules should be homogeneous owing to the rather small amount of $PC_{71}BM$ in the active layer. Therefore, the value of η_{D} can be considered to be the same in different active layers. The photogenerated electron volume density can be simply estimated by

$$\rho(\lambda) \propto \frac{|E(\lambda)|^2}{h\nu} \eta_{\mathrm{A}}(\lambda). \tag{2}$$

If the distributions of donors and acceptors in the blend films are homogeneous, then $\eta_{\mathrm{A}}(\lambda)$ is kept constant in the whole active layer for the same incident light. Therefore, the photogenerated electron distribution can be estimated according to the optical field distribution and the absorption coefficients of the blend films, as exhibited in Figs. 4(b), 4(d), and 4(f). For the photogenerated electron distribution images, the black region represents the large photogenerated electron volume density. According to the above analysis, the photogenerated electron volume density near the Al electrode plays a crucial role in determining hole injection from the Al electrode under light illumination. The obvious dip in the EQE spectra can be well explained by the relatively low photogenerated electron volume density in this spectral range. Meanwhile, the EQE spectral shape of PPDs becomes flatter as the PBDT-TS1 doping ratio is increased, which can be well explained by the more continuous photogenerated electron distribution near the Al electrode.

Based on the above analysis, the major charge carriers in the PPDs should be the holes injected from the Al electrode under light illumination. Therefore, hole transport in the active layers should play a key role in determining the EQE values. It is known that the EQE values can also be calculated according to the number of charge carriers flowing across the photodetector per incident photon, as expressed by[20,25]

$$\mathrm{EQE} \propto \frac{\chi\tau}{T} = \frac{\chi\tau\mu V}{L^2}, \tag{3}$$

where χ is the fraction of excitons that dissociated into electrons and holes, τ is the lifetime of trapped electrons, T is the transport time of a hole flowing across the active layer, V is the applied bias, L is the active layer thickness, and μ is the hole mobility. It is well known that the hole transport time for flowing across the active layer should decrease with increasing bias. To further investigate the effect of the PBDT-TS1 doping ratio on hole transport in the active layer, a series of hole-only devices was fabricated with a structure comprising ITO/PEDOT:PSS/active layers/MoO_3/Ag. The J–V curves of all the hole-only devices were measured in dark conditions, and the square root of the current density versus voltage ($J^{1/2}$–V) curves are shown in Fig. 5. It is apparent that hole transport in ternary active layers markedly decreases with increasing PBDT-TS1 doping ratio in donors. Meanwhile, hole tunnelling injection may be weakened by the increased number of shallower electron traps in the ternary active layer. According to previous reports, the hole mobility of PBDT-TS1 is $\sim 1.09 \times 10^{-2}$ $\mathrm{cm^2 \cdot V^{-1} \cdot s^{-1}}$, which is much

larger than that of P3HT (2×10^{-4} cm^2·V^{-1}·s^{-1}).[26,27] However, the current density of P3HT:PC_{71}BM-based devices is larger than that of PBDT-TS1:PC_{71}BM-based devices, which is mainly attributed to the relatively large hole injection barrier from the ITO electrode onto the HOMO of PBDT-TS1. This phenomenon indicates that the interfacial barrier plays a crucial role in determining hole injection from the external circuit. It is obvious that the current density of hole-only devices decreases with increasing PBDT-TS1 doping ratio in donors, even more than that of devices with PBDT-TS1:PC_{71}BM as an active layer. The decreased current density of hole-only devices can be ascribed to the disrupted hole transport channels in the ternary active layer. The energy barrier of 0.2 eV between HOMOs of P3HT and PBDT-TS1 may limit hole transport in the ternary active layer, resulting in the decreased EQE of ternary PPDs.

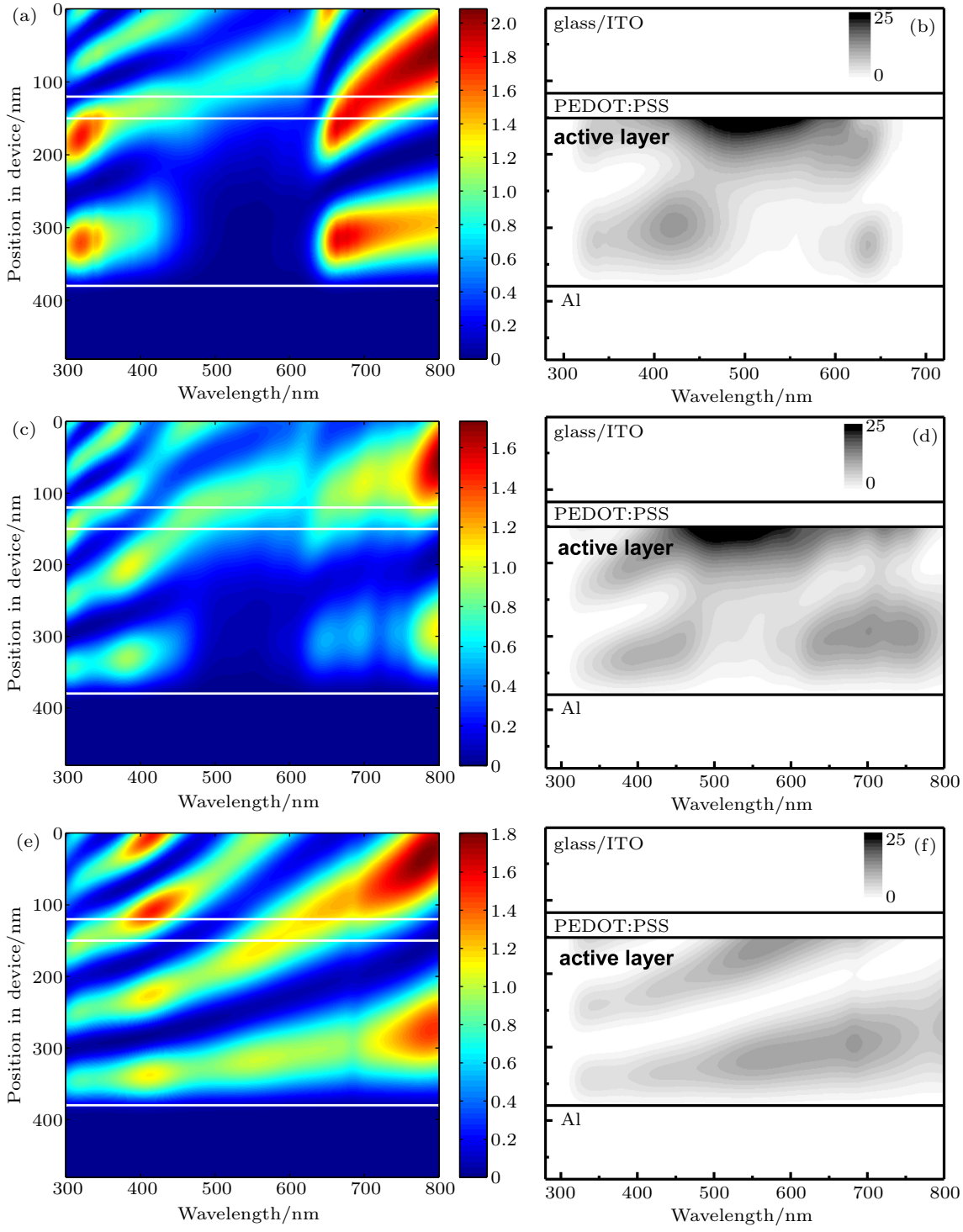


Fig. 4. (color online) Optical field distribution and photogenerated electron volume density in the active layers of PPDs with ((a), (b)) P3HT:PC_{71}BM (100:1), ((c), (d)) P3HT:PBDT-TS1:PC_{71}BM (50:50:1), and ((e), (f)) PBDT-TS1:PC_{71}BM (100:1) as the active layers.

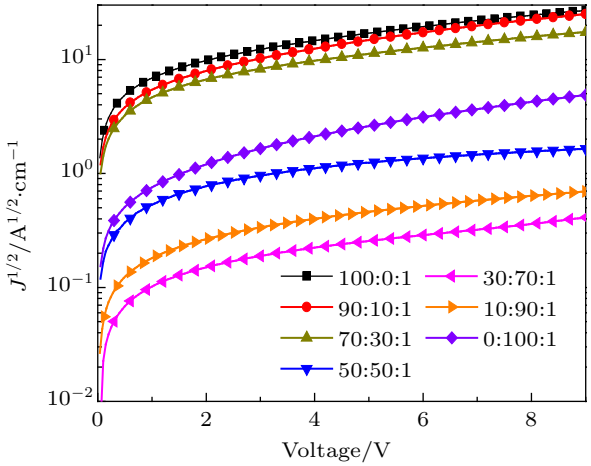


Fig. 5. (color online) $J^{1/2}$–V curves of hole-only devices with ITO/PEDOT:PSS/active layers/MoO_3/Ag with different PBDT-TS1 doping ratios.

To further clarify the working mechanism of PPDs containing different PBDT-TS1 doping ratios in donors, the current density versus voltage (J–V) curves under 625-nm light illumination with an intensity of 8.07 μW/cm^2 and 760-nm light illumination with an intensity of 5.94 μW/cm^2 and in the dark were measured, respectively. The selected 625- or 760-nm illumination light is based on the best EQE values of PPDs under light illumination. The photocurrent densities (J_{ph}) were calculated according to the J–V curves in the dark and under 625-nm light illumination, as shown in Fig. 6(a). It is apparent that the J_{ph} value of PPDs continuously decreased with increasing PBDT-TS1 doping ratios up to 90 wt% in donors, which is attributed to the increased hole injection barrier and disrupted hole transport channel in the ternary active layers. The PPDs with PBDT-TS1:$PC_{71}BM$ (100 : 1 wt/wt) as active layers exhibit a relatively large J_{ph} owing to the enhanced hole transport along with PDBT-TS1 channels in the binary active layer. The J_{ph}–V curves for PPDs under 760-nm light illumination are shown in Fig. 6(b). The PPDs with P3HT:$PC_{71}BM$ (100 : 1 wt/wt) as the active layer exhibit a rather low J_{ph} owing to the fewer trapped electrons in $PC_{71}BM$ near the Al electrode, resulting from the rather low photon harvesting of P3HT in this spectral range. It is apparent that the J_{ph} value of PPDs markedly increases by doping PBDT-TS1 in the active layer under 760-nm light illumination, which is mainly attributed to the contribution of PBDT-TS1 photon harvesting of the trapped electrons in $PC_{71}BM$ near the Al electrodes. The J_{ph} variation of PPDs is in accordance with the observed EQE spectra of PPDs with different PBDT-TS1 doping ratios in donors.

In addition to the EQE values, response range, and speed of PPDs, the responsivity (R) and specific detectivity (D^*) are also key parameters for evaluating PPD performance. R and D^* values of typical PPDs with $P3HT_{100-x}$:PBDT-$TS1_x$:$PC_{71}BM_1$ as active layers ($x = 0$, 50, 100) were calculated under −10 V bias according to

$$R = \frac{J_{ph}}{I_{in}}, \tag{4}$$

$$D^* = \frac{R}{\sqrt{2eJ_d}}, \tag{5}$$

where I_{in} is the incident light intensity, J_d is the dark current density, and e is the absolute value of the electron charge.[28,29]

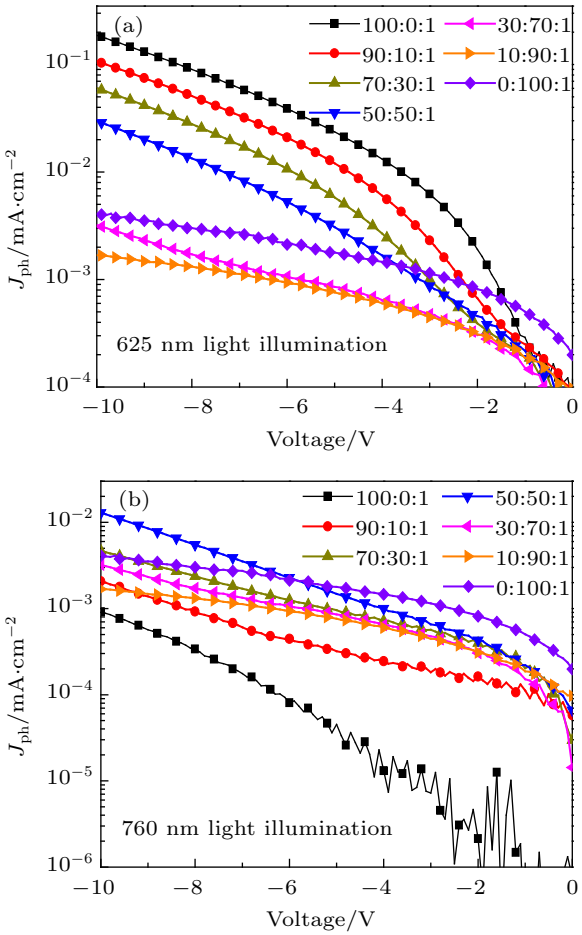


Fig. 6. (color online) J–V curves of PPDs with different PBDT-TS1 doping ratios in donors under different light illumination: (a) 625-nm light illumination with an intensity of 8.07 μW/cm^2; (b) 760-nm light illumination with an intensity of 5.94 μW/cm^2.

The R and D^* spectra of typical PPDs with $P3HT_{100-x}$:PBDT-$TS1_x$:$PC_{71}BM_1$ as active layers ($x = 0$, 50, and 100) under −10 V bias were calculated and are shown in Fig. 7. It is apparent that P3HT:$PC_{71}BM$-based PPDs exhibit the highest EQE, R, and D^* values in the short-wavelength range; the corresponding values are rather low in the NIR owing to the absence of photon harvesting. The three key parameters in the short-wavelength range all markedly decrease with increasing PBDT-TS1 doping ratio in donors, which can be well explained by the decreased hole transport ability and weakened hole injection from the external circuit. The EQE, R, and D^* values of PPDs with $P3HT_{50}$:PBDT-$TS1_{50}$:$PC_{71}BM_1$ as active layers obviously improved in the

NIR, which can be attributed to photon harvesting of PBDT-TS1. For PBDT-TS1:$PC_{71}BM$-based PPDs, R and D^* values were lower than those of the optimised ternary PPDs in the whole spectral range. The low R and D^* values can be attributed to the limited hole tunnelling injection from Al onto the HOMO of PBDT-TS1. Experimental results indicate that the energy levels, absorption coefficients, and charge mobility of the materials used are the key parameters for obtaining highly sensitive PM-type NIR PPDs.

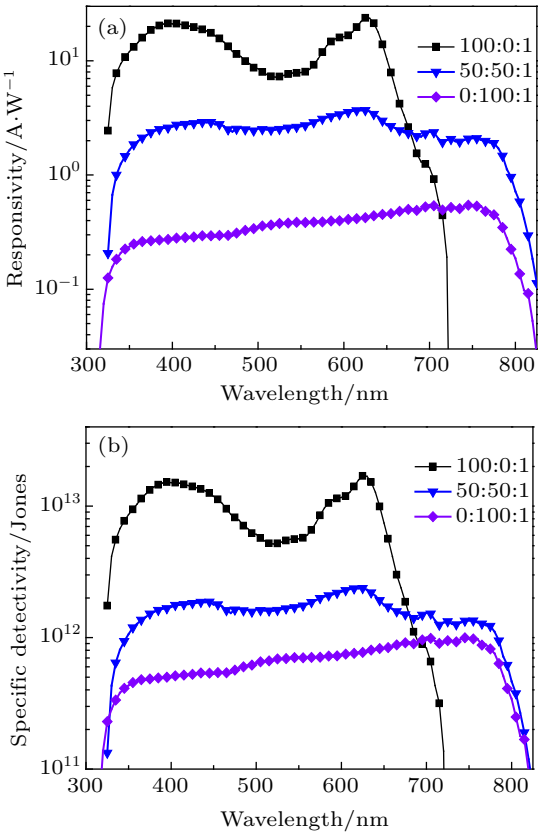


Fig. 7. (color online) (a) Responsivity and (b) specific detectivity spectra of PPDs with $P3HT_{100-x}$:PBDT-$TS1_x$:$PC_{71}BM_1$ as active layers ($x = 0$, 50, 100) under -10 V bias.

4. Conclusions

A series of high-performance PM-type PPDs was fabricated with $P3HT_{100-x}$:PBDT-$TS1_x$:$PC_{71}BM_1$ as the active layers. The spectral response range of PM-type PPDs can be extended to the NIR by adjusting the PBDT-TS1 doping ratio in donors. The EQE, R, and D^* values of PPDs strongly depend on the interfacial band bending and hole mobility in the active layers. The best EQE values of PPDs with $P3HT_{50}$:PBDT-$TS1_{50}$:$PC_{71}BM$ as the active layers reach 830%, 720%, and 330% under 390-, 625- and 760-nm light illumination and -10 V bias, respectively. We proposed a simple method to prepare high-performance NIR PPDs by doping narrow-bandgap material in the active layers.

References

[1] Yang D Z, Zhou X K, Wang Y P, Vadim A, Alshehri S M, Ahamad T and Ma D G 2016 *J. Mater. Chem. C* **4** 2160
[2] Wang X, Li H F, Su Z S, Fang F, Zhang G, Wang J B, Chu B, Fang X, Wei Z P, Li B and Li W L 2014 *Org. Electron.* **15** 2367
[3] Yang D, Yang S Y, Zhang L and Zou B S 2015 *Acta Phys. Sin.* **64** 108503 (in Chinese)
[4] Wang T H, Chen C B, Guo K P, Chen G, Xu T and Wei B 2016 *Chin. Phys. B* **25** 038402
[5] Xiong S X, Tong J H, Mao L, Li Z F, Qin F, Jiang F Y, Meng W, Liu T F, Li W W and Zhou Y H 2016 *J. Mater. Chem. C* **4** 1414
[6] Guo J C, Zuo Y H, Zhang Y, Ding W C, Cheng B W, Yu J Z and Wang Q M 2009 *Chin. Phys. B* **18** 02223
[7] Liu C, Wang K, Gong X and Heeger A J 2016 *Chem. Soc. Rev.* **45** 4825
[8] Su Z S, Hou F H, Wang X, Gao Y, Jin F M, Zhang G, Li Y T, Zhang L G, Chu B and Li W L 2015 *ACS Appl. Mater. & Interfaces* **7** 2529
[9] Keivanidis P E, Ho P K H, Friend R H and Greenham N C 2010 *Adv. Funct. Mater.* **20** 3895
[10] Gong X, Tong M H, Xia Y J, Cai W Z, Moon J S, Cao Y, Yu G, Shieh C L, Nilsson B and Heeger A J 2009 *Science* **325** 1665
[11] Ramuz M, Bürgi L, Winnewisser C and Seitz P 2008 *Org. Electron.* **9** 369
[12] Li L L, Zhang F J, Wang W B, An Q S, Wang J, Sun Q Q and Zhang M 2015 *ACS Appl. Mater. & Interfaces* **7** 5890
[13] Li L L, Zhang F J, Wang J, An Q S, Sun Q Q, Wang W B, Zhang J and Teng F 2015 *Sci. Rep.* **5** 9181
[14] Pan Y L, Cobler P, Rhodes S, Potter A, Chou T, Holler S, Chang R K, Pinnick R G and Wolf J P 2001 *Rev. Sci. Instrum.* **72** 1831
[15] Hayden O, Agarwal R and Lieber C M 2006 *Nat. Mater.* **5** 352
[16] Knupfer M 2003 *Appl. Phys. A* **77** 623
[17] Reynaert J, Arkhipov V I, Heremans P and Poortmans J 2006 *Adv. Funct. Mater.* **16** 784
[18] Hiramoto M, Imahigashi T and Yokoyama M 1994 *Appl. Phys. Lett.* **64** 187
[19] Chen H Y, Lo M K F, Yang G W, Monbouquette H G and Yang Y 2008 *Nat. Nanotech.* **3** 543
[20] Guo F W, Yang B, Yuan Y B, Xiao Z G, Dong Q F, Bi Y and Huang J S 2012 *Nat. Nanotech.* **7** 798
[21] Wang W B, Zhang F J, Li L L, Zhang M, An Q S, Wang J and Sun Q Q 2015 *J. Mater. Chem. C* **3** 7386
[22] Li Y, Huang H, Wang M J, Nie W Y, Huang W X, Fang G J and Carroll D L 2012 *Sol. Energy Mater. Sol. C* **98** 273
[23] Burkhard G F, Hoke E T and McGehee M D 2010 *Adv. Mater.* **22** 3293
[24] Armin A, Velusamy M, Wolfer P, Zhang Y L, Burn P L, Meredith P and Pivrikas A 2014 *ACS Photonics* **1** 173
[25] Saran R, Stolojan V and Curry R J 2014 *Sci. Rep.* **4** 934
[26] Zhang S Q, Uddin M A, Zhao W C, Ye L, Woo H Y, Liu D L, Yang B, Yao H F, Cui Y and Hou J H 2015 *Polym. Chem.* **6** 2752
[27] Sirringhaus H, Brown P J, Friend R H, Nielsen M M, Bechgaard K, Langeveld-Voss B MW, Spiering A J H, Janssen R A J, Meijer EW, Herwig and Amp P 1999 *Nature* **401** 685
[28] Wang W B, Zhang F J, Bai H T, Li L L, Gao M L, Zhang M and Zhan X W 2016 *Nanoscale* **8** 5578
[29] Liu C, Wang K, Yi C, Shi X J, Du P C, Smith A W, Karim A and Gong X 2015 *J. Mater. Chem. C* **3** 6600